Reactivity of supported metal clusters: the reduction of NO by CO on a Pd/MgO(100) model catalyst

2002 J. Phys.: Condens. Matter 14 4251

(http://iopscience.iop.org/0953-8984/14/16/315)

INSTITUTE OF PHYSICS PUBLISHING JOURNAL OF PHYSICS: CONDENSED MATTER

J. Phys.: Condens. Matter **14** (2002) 4251–4269 PII: S0953-8984(02)31799-5

Reactivity of supported metal clusters: the reduction of NO by CO on a Pd/MgO(100) model catalyst

G Prévot[1], O Meerson, L Piccolo[2] and C R Henry[3]

CRMC2[4]-CNRS, Campus de Luminy, Case 913 13288 Marseille cedex 09, France

E-mail: henry@crmc2.univ-mrs.fr

Received 11 December 2001
Published 11 April 2002
Online at stacks.iop.org/JPhysCM/14/4251

Abstract

In order to bridge the 'material gap' in heterogeneous catalysis it is shown that supported model catalysts can be used. They are prepared by epitaxial growth on an oxide single crystal. This work describes results obtained with Pd clusters supported on MgO(100) surfaces as a model catalyst for the reduction of NO by CO. The morphology of the Pd particles was analysed by transmission electron microscope. By using molecular beam techniques it was possible to determine the elementary steps of the reaction and the reaction mechanism. It is shown that the dissociation of NO is the key step for the reaction. After dissociation, two types of adsorbed nitrogen atom are obtained: a strongly bound one that does not desorb during the reaction and a loosely bound one that desorbs associatively. Oxygen atoms resulting from the NO dissociation react with adsorbed CO or diffuse in the lattice of the Pd particles. The reaction rate depends on both the particle size and the particle morphology. The reaction kinetics is also influenced by the support via the capture, by the metallic particles, of the reactants physisorbed on the support.

1. Introduction

The basic mechanisms of heterogeneous catalysis are conveniently studied by surface science techniques under ultra-high-vacuum (UHV) conditions. However, compared with industrial catalysis two gaps have been pointed out. The first one is called the 'material gap'. It expresses the material complexity of technical catalysts compared with model catalysts that are used by surface scientists. Indeed technical catalysts are made of nanometric metallic particles prepared

[1] Present address: GPS, UMR CNRS 7588, Universités Paris 6 et 7, Tour 23, 2 place Jussieu, 75251 Paris cedex 05, France.
[2] Present address: IRC-CNRS, 2 Avenue Albert Einstein, 69626 Villeurbanne cedex, France.
[3] Author to whom any correspondence should be addressed.
[4] Associated with the Universities of Aix-Marseille II and III.

0953-8984/02/164251+19$30.00

by wet impregnation on oxide powders, while most of the model catalysts that are studied by surface science techniques are single crystals exposing a well defined crystal plane on the top surface. It is clear that this type of model catalyst plays a major role in the elucidation of the mechanisms of catalytic reactions [1]. However, it cannot take into account the finite size of the metal particles and the presence of the support, which are known to influence, to some extent, the catalytic activity and the detailed reaction mechanism [2]. In order to bridge this material gap several surface science groups now work with a new type of model catalyst made, like technical catalysts, of nanometric metal particles, but these particles are prepared *in situ*, under UHV, on extended crystalline oxide surfaces and exhibit well defined size and morphology. Several reviews have recently appeared on the work performed on these supported model catalysts [3–5]. The second gap, called the 'pressure gap', is due to the fact that technical catalysis takes place around atmospheric pressure, that corresponds to a ten orders of magnitude higher pressure than in the UHV conditions that are generally used in surface science. To close this gap several new techniques have been recently introduced allowing us to work on model catalysts under high pressure. These new techniques are, for example, sum frequency generation [6], polarization modulation infrared spectroscopy [7], high-pressure STM [8] and x-ray diffraction.

In this paper, we shall address the bridging of the material gap. More precisely we shall see how the particle size and morphology of the catalyst particles as well as the support may influence the reaction kinetics. For this purpose we shall take the example of the NO reduction by CO on a Pd/MgO(100) model catalyst. NO reduction by CO is the most important reaction taking place in a car exhaust catalytic converter, that removes the CO and NO toxic gases. The catalysts are a mixture of noble metals such as Pt, Pd and Rh supported on alumina doped by other oxides. Rh is the most active metal to remove nitrogen oxides. However, due to its very high price, it should be suitable to replace it by Pd, which is much cheaper. In recent years several surface science studies have been undertaken on Pd single crystals to try to understand the mechanism of the CO–NO reaction [9–16]. It was shown by Goodman's group that the (111) surfaces are more active than more open ones such as (100) and (110) [12, 14, 15]. These single-crystal studies have demonstrated that the reaction takes place after chemisorption of CO and NO but two different mechanisms have been proposed for the reaction: (i) direct reaction between CO and NO, giving CO_2 and adsorbed N [11]; (ii) dissociation of NO followed by the formation of CO_2 while an adsorbed nitrogen adatom recombines with another one to give a nitrogen molecule or reacts with an adsorbed NO molecule giving N_2O [12–15]. In the case of mechanism (ii) the selectivity in dinitrogen is higher on the more open surfaces [12]. Recently several studies have been published on supported model catalysts by Goodman's group on Pd/alumina [15] or Pd/silica [17] and by our group on Pd/MgO [18, 19]. These studies have shown that the NO reduction by CO depends on particle size and morphology and that the support plays an important role in the reaction kinetics. In this paper we shall review, from previous and new results, how the structure of the model catalysts can be characterized by transmission electron microscope (TEM) and how the elementary steps as well as the reaction mechanism can be studied using molecular beam techniques.

2. Experiment

The Pd particles are grown *in situ*, under UHV, in the reaction chamber by condensing a calibrated beam of Pd (2×10^{13} atoms cm^{-2} s^{-1}) on an MgO(100) surface at 400–450 °C. The MgO crystals are either cleaved *in situ* or in air and subsequently cleaned under vacuum [18]. The cleanness of the sample was checked by Auger electron spectroscopy. The adsorption of CO and NO has been studied by using a pulsed supersonic molecular beam impinging on the

sample. The detection of desorbed products was achieved by a differentially pumped mass spectrometer. The set-up has been described previously [20]. The intensity of the beam at the sample level was 2×10^{13} and 1.9×10^{13} molecules cm^{-2} s^{-1} for CO and NO, respectively. During the reaction a molecular beam of CO or NO was used and the other reactant (^{15}NO or ^{13}CO) was provided as an isotropic pressure through a leak valve. After the reactivity measurements the sample was covered by a thin carbon film, which was later floated in dilute HCl and mounted on a copper electron microscopy grid. The carbon film containing the Pd particles was observed with a Jeol 2000FX TEM operated at 200 kV.

3. Structure and morphology of the Pd particles

The nucleation and growth of the metal particles is controlled mainly by three parameters: the deposition rate, the deposition time and the sample temperature. The saturation density of clusters depends strongly on the sample temperature and can be continuously varied between 1×10^{10} and 5×10^{12} clusters cm^{-2} [4]. The cluster size varies as a power law of the deposition time. The exponent lies between 0.29 and 0.39, depending on the substrate temperature and cluster density [21]. The morphology of the particles is, as we shall see, a crucial parameter in the reactivity of supported model catalysts but it is the most difficult to control. In fact the morphology of the metal particles is generally governed by kinetics and thus it can change considerably with the experimental growth conditions [22]. However, at very low deposition rate and at high temperatures the shape of the grown particles becomes close to the equilibrium one [23]. The equilibrium shape of a supported crystal is a universal shape (e.g. a truncated octahedron for an fcc crystal), which is truncated at the interface in proportion to the adhesion energy [22]. However, calculations show that this is true only if there is no lattice mismatch between the deposited crystal and the support; in the opposite case the particle shape depends on the particle size [24]. Indeed, the shape of the Pd particles supported on MgO(100) depends on the particle size below 10 nm [25]. At and above 10 nm the interfacial strain due to the misfit is relaxed by dislocations and the equilibrium shape no longer evolves.

Figure 1 shows the TEM characterization of a typical Pd deposit corresponding to 10 min of deposition at 450 °C on a UHV-cleaved MgO substrate. Picture (*a*) shows that the particles have a square outline. All the squares have the same orientation due to epitaxial growth. The electron diffraction pattern (*b*) indicates that the Pd particles are in the (100) epitaxy. The size distribution is nearly Gaussian, with a mean value of 15.2 nm and a standard deviation of 20%. Some particles are elongated due to coalescence of two neighbouring particles. The three-dimensional shape of the particles, if they are larger than about 6 nm, can be obtained by the weak-beam dark-field imaging technique, that produces thickness fringes [23]. TEM views in two perpendicular directions (top view + cross section) are also a very convenient and accurate means to characterize the morphology. Figures 2(*a*) and (*b*) show such views of Pd particles prepared at high temperature on UHV-cleaved MgO substrates. From these views, one can derive the morphology of the particles, that is a truncated octahedron exposing (111) and (100) facets as schematically represented in figures 2(*c*) and (*d*). The profile view shows clearly the presence of re-entrant angles at the interface due to a wetting angle larger than 90°. It is worth noting that such re-entrant angles cannot be seen in a TEM top view with either STM or AFM techniques. The measurement of the actual interface area is particularly important if one wishes to derive the adhesion energy [23]. In figure 2(*a*), the (200) lattice fringes are seen, indicating that the edges of the square base of the particles are parallel to the ⟨110⟩ directions of the Pd lattice. The top (100) facet can be distinguished by a different contrast. These Pd particles were exposed in majority (111) facets. From these measurements it is possible to derive the exposed Pd area, that is important to determine the adsorbate coverage and the turnover frequency in

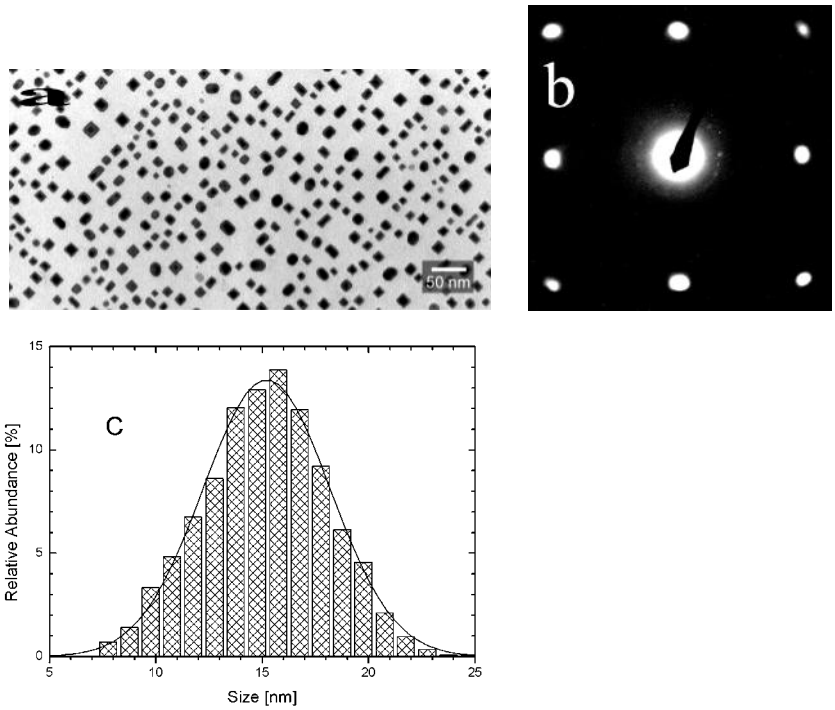

Figure 1. TEM characterization of a Pd/MgO(100) model catalyst obtained by a 10 min exposition of a UHV-cleaved MgO crystal to the Pd flux at 450 °C. (*a*) Large-area micrograph. (*b*) Electron diffraction diagram. (*c*) Size histogram.

reactivity experiments. On air-cleaved surfaces, the density of defects is much higher and thus so is the density of clusters which nucleate on defects [4]. Then, for a thick deposit most of the particles have coalesced during growth and the particles no longer retain the equilibrium shape: the top (100) facets are dominant in this case as shown in figure 3 and in a previous study [18]. AFM [26] and STM [27] can provide *in situ* complementary information on such model catalysts, such as the atomic structure of the facets. STM can be used on very thin oxides that are insulating in the bulk such as alumina [28] or on oxides with a smaller gap such as TiO_2 [3].

4. NO adsorption

4.1. NO dissociation

NO adsorption has been previously studied by the pulsed molecular beam technique [29]. In this technique, a molecular beam pulse is sent onto the sample and we measure, as a function of time by mass spectrometry, the different products desorbing simultaneously from the sample surface. It was shown that NO is physisorbed or reflected from the clean MgO surface. On the Pd particles, NO is first molecularly chemisorbed, and part of it dissociates if the coverage is not too high. The simultaneous production of dinitrogen proved that the association reaction of two adsorbed nitrogen atoms is fast, with a kinetics close to that of NO desorption. On a fresh (i.e. never exposed to NO) sample, the dissociation rate is very large and after several pulses (corresponding to a total exposure of about 10 min, equivalent to 30 L) the dissociation rate remains constant (i.e. the desorbed pulses are stationary).

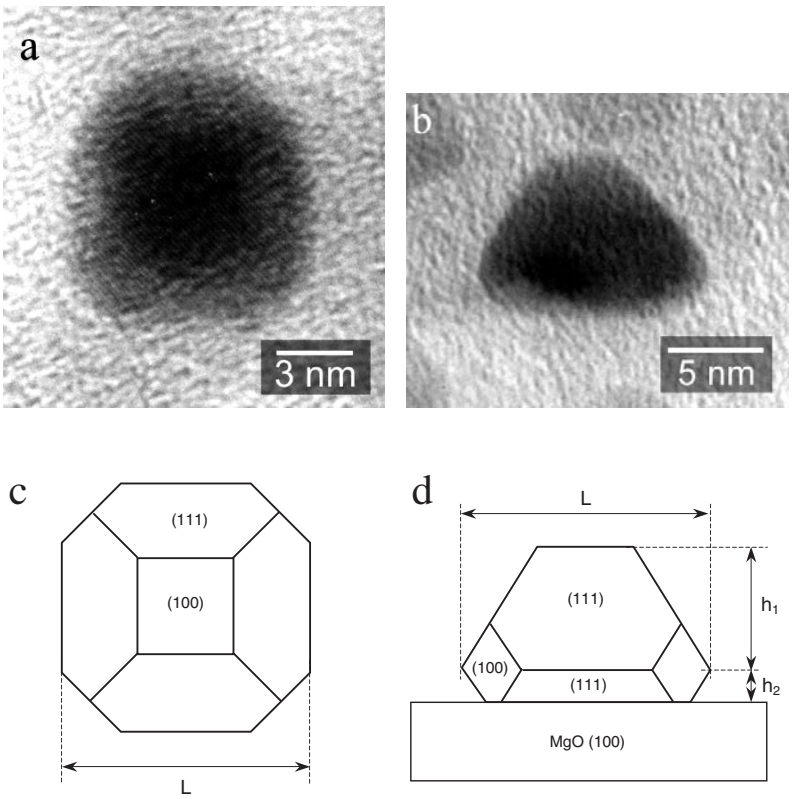

Figure 2. TEM determination of the morphology of Pd particles epitaxially grown at high temperature on UHV-cleaved MgO(100). (*a*) HRTEM top view of a Pd truncated octahedron. (*b*) Profile view of a Pd truncated octahedron. (*c*), (*d*) Schematic representation of a truncated octahedron Pd particle in top view and in profile view, respectively. The aspect ratio (L1 + L2)/L is 0.69.

We have performed new experiments to see what happens for the oxygen resulting from the dissociation of NO. First, no oxygen molecule was observed to desorb. In fact on Pd extended surfaces oxygen associatively desorbs near 530 °C, that is higher than the temperature range used for our studies of the CO–NO reaction (150–450 °C) [30–32]. If oxygen atoms remain on the Pd surface they should be seen by dosing with CO to form CO_2. In a first type of experiment, using an NO beam (see figure 4), one compares the first desorbing pulse of NO with the stationary one, which shows only reversible dissociation of NO (curves 1 and 2). By reversible dissociation we mean that there is no accumulation of the dissociation products, otherwise we could not obtain a stationary state for the desorbed pulses. Then, the sample is exposed for 5 min at 330 °C to 30 L of CO and a pulse of NO is sent to the sample. The desorbed NO pulse (3) is nearly identical to the stationary one. This experiment shows that the adsorption capacity of NO has not increased; in other words adsorbed oxygen was not blocking some of the NO dissociation sites. In order to clarify this point a second type of experiment has been performed using a CO beam. The sample was now exposed to 15 L of ^{15}NO at 250 °C, then a CO pulse was sent to the sample after a waiting time Δt (after the closing of the NO leak valve) while the CO_2 production was measured by the mass spectrometer. Figure 5 shows that CO_2 was effectively produced due to the presence of adsorbed oxygen, but its

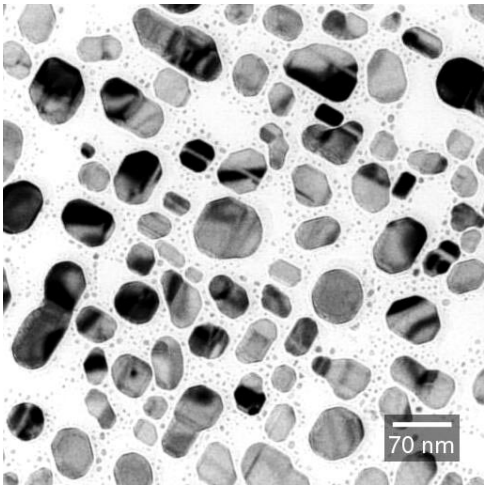

Figure 3. TEM picture of a thick Pd deposit on an air-cleaved MgO(100) substrate showing coalesced particles with a mean size of 45 nm exposing large (100) top facets.

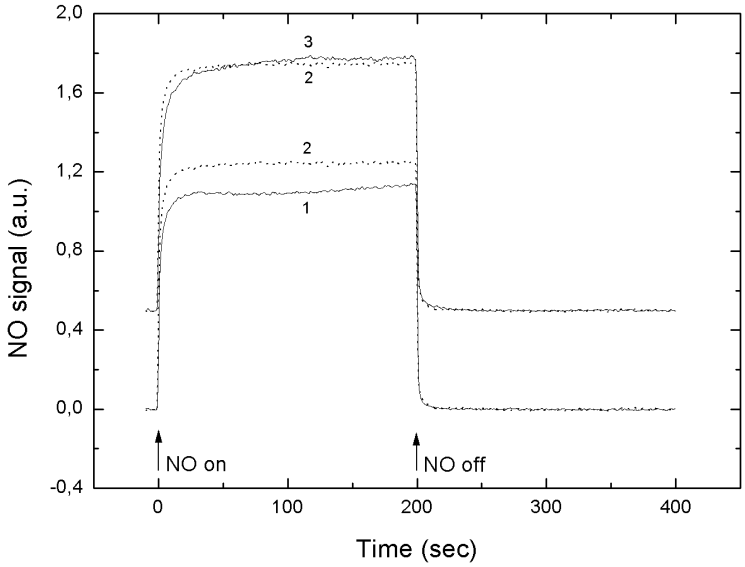

Figure 4. NO adsorption–desorption transients on a Pd/MgO(100) model catalyst at 330 °C. (1) First NO pulse from the fresh sample. (2) Stationary NO pulse. (3) NO pulse after exposition of 30 L of CO.

quantity decreased with increasing waiting time. The same experiments have been performed at several temperatures between 225 and 300 °C. The maximum (i.e. initial) coverage of oxygen was the largest at 250 °C, which corresponds to the maximum rate of the CO–NO reaction. The decrease of adsorbed oxygen with waiting time is accelerated by increasing the temperature. If one attempts to fit the temperature dependence of the characteristic time with an Arrhenius law, one obtains a very small activation energy of 2.3 kcal mol^{-1}, with a prefactor of 5×10^{-2} s^{-1}. This indicates that the overall process cannot be modelled by a single elementary step. The only possible explanation of the decay of the adsorbed oxygen on the Pd particles is the

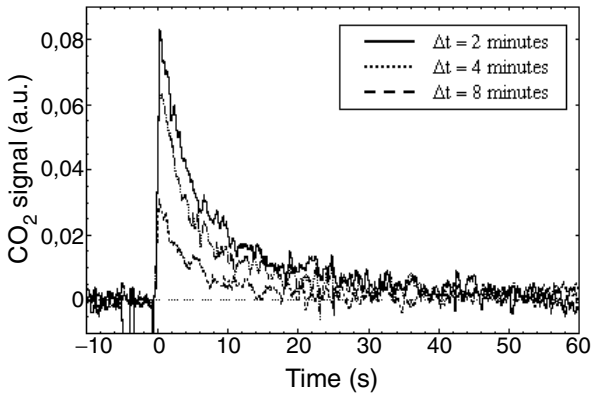

Figure 5. Series of CO_2 pulses obtained at 250 °C by reaction of the CO molecular beam with adsorbed oxygen for various waiting times after the exposition to 15 L of NO at the same temperature.

diffusion of oxygen inside the Pd particles. This second experiment also explains why, in the first experiment, adsorbed oxygen did not block the adsorption capacity of NO (at 330 °C the oxygen has rapidly diffused in the Pd particles). So, what blocks the NO dissociation capacity? The only possibility is to have a strongly bound nitrogen species that does not desorb at the temperature where the reaction occurs. In fact, this kind of strongly adsorbed nitrogen has been already proposed by Goodman and co-workers [14, 17]. They observed by TPD that two kinds of nitrogen species were adsorbed, one desorbing near 230–280 °C and the other one near 330–430 °C. The strongly bound species does not recombine or react with adsorbed oxygen in the temperature window of the reaction. On the contrary, it acts as a poison for further NO dissociation. In order to measure the steady-state coverage of oxygen during reaction, we have performed a third type of experiment. The steady state of the reaction is established with a CO beam and an isotropic pressure of NO, then the CO beam is interrupted for a time Δt before that the CO beam is again turned on, while the production of CO_2 is measured (see figure 13). With these measurements we determine that the steady-state coverage of oxygen (at 250 °C and for an NO pressure of 1×10^{-7} Torr) was of the order of 10^{-3} ML during the reaction. When the CO beam was turned off, the oxygen coverage increased and reached a new steady state (at zero CO pressure) of about 10^{-2} ML. This corresponds to the equilibrium between the dissociation of NO and the diffusion of oxygen into the bulk of the particles. The kinetic to establish the new equilibrium is not very fast (the relaxation time is 22 s at 250 °C).

The stationary state dissociation rate of NO, that we call reversible, has been previously measured [29]. It increases with substrate temperature (from 150 to 450 °C). It also depends on particle size (from 2.8 to 15.6 nm) [29]. From this study the (reversible) dissociation rate increases with particle size but decreases again for very large particles. In fact this drop was rather a morphology effect than a size effect (see discussion). Indeed TEM characterization showed that the small and medium-sized particles had a truncated octahedron shape exhibiting mostly (111) facets (see figure 2) while the large ones were coalesced and exposed mainly (100) facets (see figure 3).

4.2. Adsorption probability

The adsorption probability can be easily measured by pulsed molecular beam experiments [29, 33]. Molecules that are scattered or desorbed from the oxide substrate have a very short

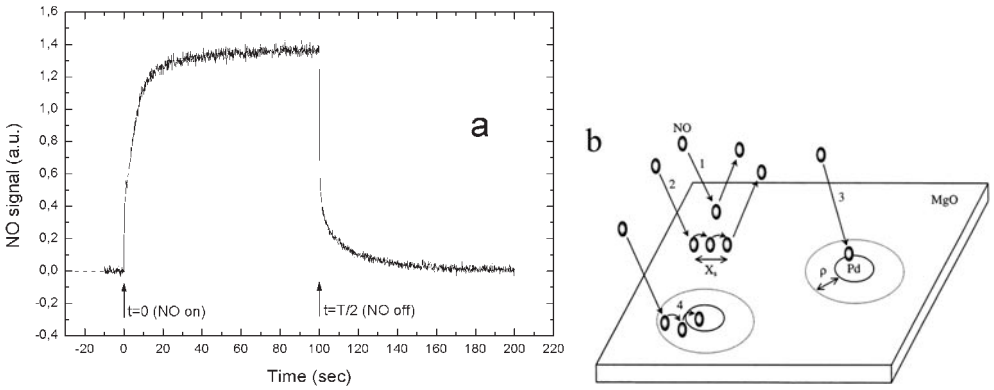

Figure 6. Adsorption of NO on a Pd/MgO model catalyst. (*a*) Typical stationary NO adsorption–desorption transient pulse. (*b*) Schematic representation of the elementary steps during the molecular adsorption of NO on a supported model catalyst: (1) quasi-elastic reflection, (2) physisorption followed by surface diffusion and desorption, (3) direct chemisorption on a Pd particle, (4) surface diffusion on the MgO support followed by capture in a chemisorbed state by a Pd particle.

residence time compared with molecules that desorb from a chemisorbed state from the metallic particles (see figure 6(*a*)). Hence, the sharp variations of the NO signal, when the NO beam is turned on or off, correspond to the first type of NO molecule (reflected or reversibly physisorbed), while the slow components originate from the second one (reversibly chemisorbed). Therefore, the amplitude of the slow component (normalized to the incident beam intensity) gives the probability for an NO molecule striking the sample to be (reversibly) chemisorbed on the Pd particles. It has been shown that this adsorption probability was increased by decreasing the substrate temperature up to saturation [29]. This saturation depends on the particle size and particle density. This phenomenon (called reverse spillover), which was observed for the first time with CO [33], is due to the capture by the Pd particles of molecules physisorbed on the oxide substrate, via surface diffusion. This mechanism is sketched in figure 6(*b*). NO molecules striking the substrate can be either immediately reflected (1) or enter a physisorbed state (2) with a probability α. Molecules impinging directly on the Pd particles are chemisorbed (3) with a probability close to unity (at low coverage). The physisorbed molecules diffuse across the substrate surface and desorb after a time τ_s (shorter than 1 μs) after travelling a mean distance X_s. During the diffusion process, if an NO molecule reaches a Pd particle it becomes chemisorbed (4). Then, one can define around each Pd particle a capture zone of width ρ. Each NO molecule that is physisorbed in the capture area will become adsorbed on the Pd particles. In a first approximation[5], ρ is equal to X_s, which is expressed by

$$X_s = a_0(\nu_{sdif}/\nu_{sad})^{1/2} \exp[(E_{sad} - E_{sdif})/2kT]. \tag{1}$$

a_0 is the distance between adsorption sites, ν_{sdif} and ν_{sad} are the frequency factors for diffusion and desorption processes and E_{sad} and E_{sdif} are the adsorption and diffusion energies of an NO molecule adsorbed on the support. From equation (1) we see that X_s increases with decreasing temperature, then we can understand that the adsorption probability also increases up to the point where the capture zones will overlap, that corresponds to saturation.

[5] Due to the interaction between the diffusion fields around neighbouring clusters the width of the capture zone decreases. A full account of this effect can be found in [33].

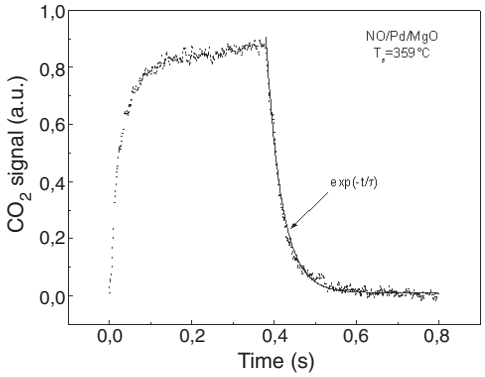

Figure 7. Measurement of the lifetime of an NO molecule on a Pd/MgO model catalyst at 359 °C by a periodic modulation of the NO molecular beam. The lifetime τ is obtained by the adjustment of the curve with an exponential decay (solid curve).

4.3. Desorption energy

The desorption energy can also be measured by the pulsed molecular beam technique [20, 29]. In the limit of low coverage, the adsorption energy is constant and the desorption follows a first-order kinetics, then when the beam is turned on or off the desorbed signal will increase or decrease exponentially with time and the time constant of the process is the lifetime of the adsorbed molecules. In the case of NO on Pd the desorption energy varies strongly with coverage, even at very low coverage [34], then during a long pulse the desorption energy varies and the signal is no longer exponential. In this case, it is necessary to modulate the beam periodically in order to obtain a weak variation of the coverage around a constant value. Thus we obtain a pseudo-first-order kinetics and the signal again varies exponentially. Such an example is shown in figure 7. From the exponential decay the lifetime can be obtained. By measuring this lifetime for different temperatures one obtains the desorption energy for the corresponding coverage (it is necessary to adjust the modulation frequency to maintain nearly the same coverage) from an Arrhenius plot of the adsorption lifetime. With this method a desorption energy of 32 kcal mole^{-1} and a frequency factor of 10^{13} s^{-1} (at a coverage between 0.02 and 0.07) have been found for Pd particles [29].

5. CO adsorption

5.1. Adsorption probability

The adsorption kinetics of CO on Pd clusters supported on MgO(100) has been previously studied by the pulsed molecular beam method [20, 33, 35]. The NO adsorption also presents the same reverse-spillover effect as CO. The adsorption probability of CO on MgO is a little weaker than for NO (0.50 instead of 0.56) and the difference $E_{sad} - E_{sdif}$ was found to be equal to 0.25 eV [33].

5.2. Desorption energy

The desorption energy of CO on Pd extended surfaces, at low coverage, varies less strongly with coverage than in the case of NO. Then, the desorption energy on Pd particles can be measured by the single-pulse method. Previous measurements have shown that the desorption energy on

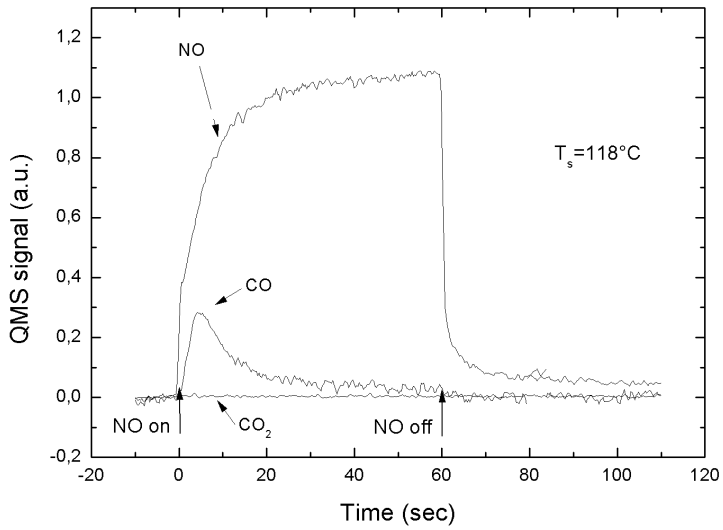

Figure 8. Adsorption–desorption of an NO pulse on a Pd/MgO model catalyst, at 118 °C, after a 3 L exposition to CO at the same temperature. NO, CO and CO_2 desorbing signals are presented.

large particles was close to 30 kcal mole^{-1} [20]. On particles smaller than 4–5 nm, at very low coverage ($\leqslant$0.01), the desorption energy was found to increase when their size decreased [35]. This increase of the desorption energy is due to a strong binding energy of CO on particle edges [4]. In contrast to NO, no dissociation of CO was observed down to 2 nm clusters [35].

For particles larger than or equal to 5 nm the adsorption energy of CO is 2 kcal mol^{-1} smaller than for NO, that means that the equilibrium coverage of CO is significantly smaller than that for NO, in the temperature window of the reaction. Another effect of this energy difference is that NO is able to displace adsorbed CO. This can be seen from the following experiment. First we expose the sample to 3 L of CO at 118 °C: at this temperature both CO and NO adsorption are only partially reversible. Then we send an NO pulse and we record the NO, CO and CO_2 desorbing from the sample (see figure 8). During the pulse of NO, some NO is desorbed but also part of the adsorbed CO is removed by NO and desorbs. No CO_2 is produced. These results show that CO can indeed be displaced by NO; in other words, the adsorption of NO is not inhibited by the presence of CO. No CO_2 was produced because the temperature is outside the reaction window; in fact NO is not dissociated at this temperature.

We have also measured the desorption kinetics of CO during the reaction by a pulsed molecular beam of CO, keeping a constant pressure of NO. The decay signal of CO is almost exponential. In figure 9 we have plotted the corresponding time constant of the CO decay (τ_{dec}) as a function of the NO pressure, at 250 °C. We can see that τ_{dec} is constant, at low pressure, and strongly decreases for NO pressures higher than 1×10^{-7} Torr. The decay of the desorbed CO signal results from the decrease of the CO coverage. It is due to the desorption of CO and also to the reaction with adsorbed oxygen. In the low-pressure limit, the time constant τ_{dec} must be equal to the true lifetime of an adsorbed CO molecule (at low coverage). At higher coverage, part of the CO is consumed by the reaction, but the adsorbed species also decrease the desorption energy of the CO molecules. Even the presence of subsurface oxygen can decrease this desorption energy [36]. All these effects lead to a decrease of τ_{dec}. In fact, from microkinetic modelling, for NO pressures larger than 5×10^{-7} Torr (at 250 °C) the total coverage (mainly NO_{ad} and O_{ad}) is larger than 0.1 [37]. From measurements, at

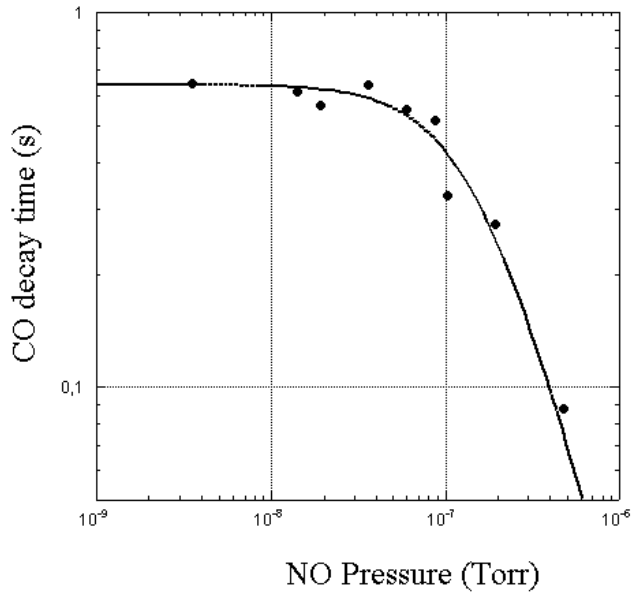

Figure 9. CO decay time constant during the CO–NO reaction at 250 °C on 10 nm Pd particles as a function of the ^{15}NO isotropic pressure after closing the CO beam. The solid curve is a guide for the eyes.

various temperatures, of τ_{dec} in the limit of low pressures of NO (where τ_{dec} is constant) we have obtained, from an Arrhenius plot, an activation energy of 27 kcal mol^{-1} and a frequency factor of 5×10^{11} s^{-1}.

6. CO–NO reaction

6.1. NO beam

The reduction of NO by CO, on Pd particles supported on MgO, has been previously studied using an NO beam and an isotropic pressure of ^{13}CO [18, 19]. It was shown that the reaction is of Langmuir–Hinshelwood type with a maximum of activity near 250 °C and that NO dissociation is a necessary step [18]. It was further demonstrated that the rate limiting step (RLS) of the reaction is the dissociation of NO at low temperature and the adsorption of CO at high temperature [19]. New results have been obtained in transient conditions. In figure 10 three series of CO_2 transients are shown for different isotropic pressures of CO, corresponding to substrate temperatures of 205, 257 and 379 °C. These three sets of curves present different behaviours. At low temperature, the time to reach the steady state is long and increases on decreasing the CO pressure. Interestingly, at the lowest pressure investigated (1×10^{-8} Torr) the CO_2 production does not decrease immediately after closing the NO beam. At this low temperature, the reaction is limited by the coverage, which is too high. After closing the NO beam, the NO coverage decreases, that either enhances the dissociation of the remaining NO adsorbed molecules or allows more CO molecules to chemisorb and react. At 257 °C, that corresponds to the maximum activity of the reaction, a transient peak is observed at high CO pressure. The fact that the maximum rate does not correspond to the steady-state ones is related to the fact that, initially at this high CO pressure, the CO coverage is close to saturation and then much larger than during the reaction at steady state. In the high-temperature regime, the time constant of the transient period becomes small and almost independent of the CO pressure.

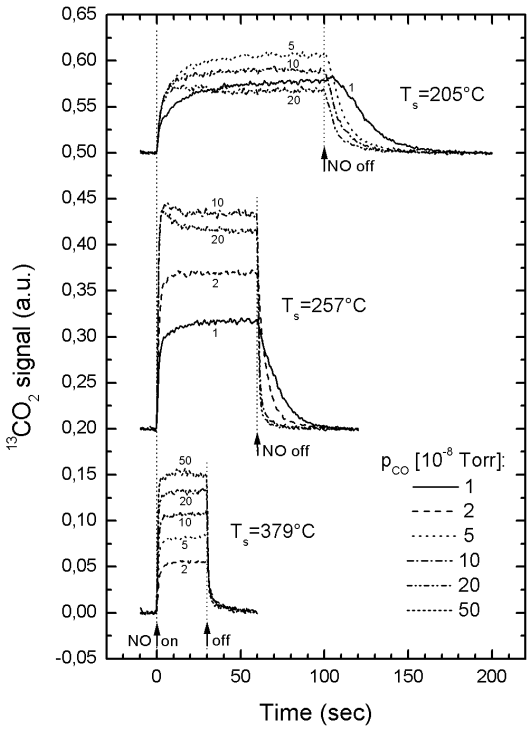

Figure 10. $^{13}CO_2$ transients during CO–NO reaction on a Pd/MgO model catalyst (2.8 nm particles) at various temperatures with various ^{13}CO isotropic pressures and a pulsed beam of NO.

These changes in the transient behaviour, which are related to changes in the relative rates of the elementary steps of the reaction, are in fact very good tests for kinetic models. The transients will be discussed in detail in a further paper on the simulation of the reaction by microkinetic modelling [37].

6.2. CO beam

The steady-state reaction rate with a CO beam and a ^{15}NO isotropic pressure (5×10^{-8} Torr) has been measured as a function of the substrate temperature (figure 11). The global shape of the curve is the same as with an NO beam [18] but the maximum reaction rate is obtained at a slightly lower temperature (near 225 °C). This difference probably reflects the uncertainties associated with the measurements of the CO and NO beam intensities and partial pressures. Figure 12 displays the reaction probability of CO as a function of the NO pressure at 250 °C. The activity increases very fast at low pressure and, beyond 1×10^{-7} Torr, it increases more slowly, due to coverage effects previously discussed, but never decreases (below 5×10^{-7} Torr). The highest reaction probability on the Pd particles is rather large (near 0.2) and comparable to that measured on Rh(111) at low pressure [38]. Figure 13 shows two transient pulses of CO_2 obtained after a closing time of the CO beam (from the steady-state conditions) of 7 and 60 s. The initial transient peak originates from the fact that the oxygen coverage is higher during NO adsorption (without CO) than during the reaction (with CO). The area of the transient peak increases with the waiting time until the steady-state oxygen coverage (in the absence of CO) is reached (see section 4.1).

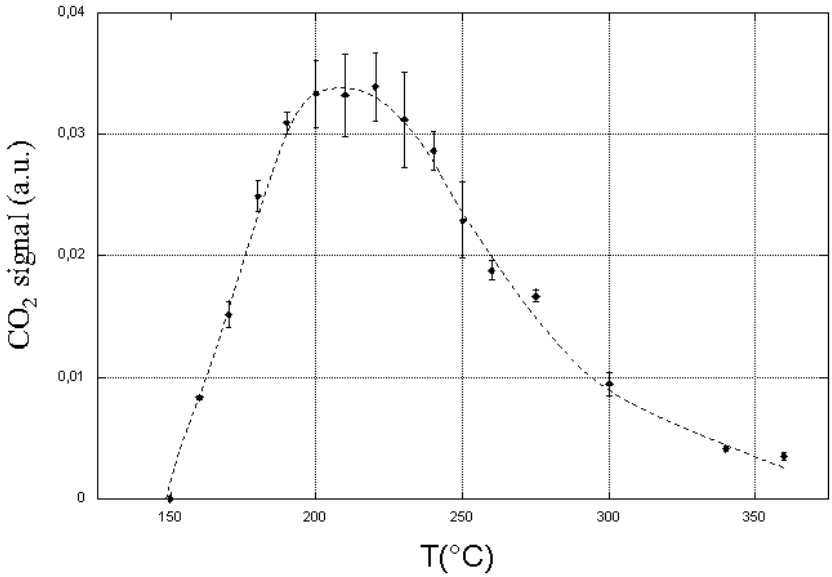

Figure 11. Steady-state production rate of CO_2 during the CO–NO reaction with a molecular beam of CO and an isotropic pressure (5×10^{-8} Torr) of ^{15}NO on 10 nm Pd particles supported on MgO(100) as a function of sample temperature.

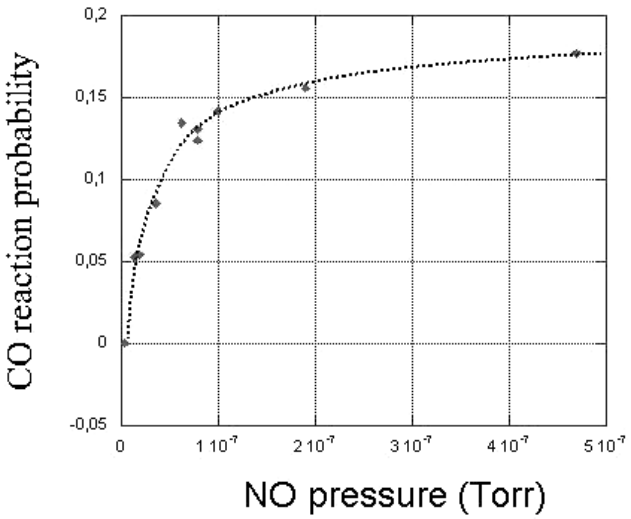

Figure 12. Reaction probability of CO at 250 °C during the CO–NO reaction with a molecular beam of CO as a function of the isotropic pressure of ^{15}NO on 10 nm Pd particles supported on MgO(100).

7. Discussion

7.1. Structure and morphology

The morphology of the supported clusters must be known if one intends to understand in detail the reaction kinetics on supported model catalysts. The morphology of a small supported crystal is only unambiguously defined at the equilibrium. The equilibrium shape of a crystal

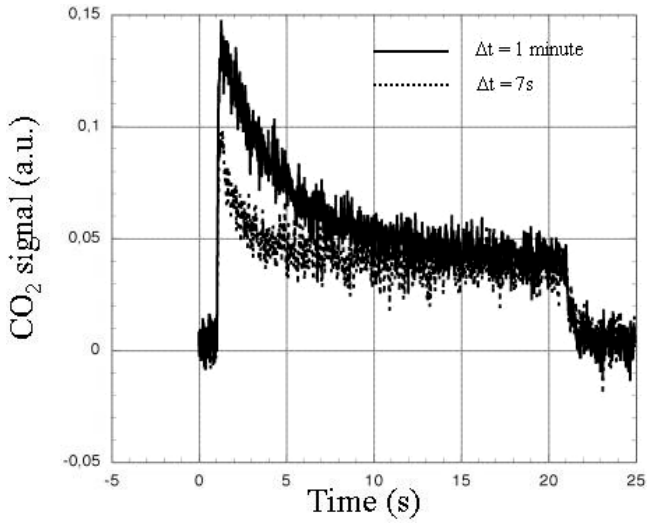

Figure 13. CO_2 transients at 250 °C for different waiting times after closing the CO beam from the steady-state conditions of the CO–NO reaction with an isotropic pressure of ^{15}NO (1×10^{-7} Torr) on 10 nm Pd particles supported on MgO(100).

is obtained by minimizing the surface energy (Wulff theorem [39]). For an fcc crystal the equilibrium shape is a cuboctahedron exhibiting only (111) and (100) facets. The extension of these two types of facet is given by the surface energy anisotropy, which is 1.15 at 0 K [40]. Increasing the temperature will result in a decrease of the surface energy anisotropy leading to a sphere, close to the melting point. It is important to note that surface energy is modified by adsorption. In the case of a different equilibrium adsorbate coverage on the different facets the surface energy, and hence the equilibrium shape, will change. In the case of oxygen adsorption, the surface energy anisotropy can be inverted on 10 nm Pd particles [23]. Therefore, during a catalytic reaction if the adsorbed coverages are not negligible (larger than about 0.1), and the temperature high enough, the shape of the catalyst particles can reversibly evolve. Thus, it is really necessary to have in the future *in situ* characterization of the morphology of metal particles during a catalytic reaction. This can now be achieved by *in situ* TEM (with a specially designed electron microscope) [41], by AFM and STM [8,42] and by GISAXS [43]. Due to the presence of the support, the equilibrium shape of a crystal is truncated at the interface in proportion to the energy of adhesion (Wulff–Kaishew theorem [44]). However, this theorem gives only the equilibrium shape for a fully relaxed crystal (i.e. no strain is present at the interface). In the presence of strain at the interface the equilibrium shape is size dependent [24]. In the case of supported Pd particles of 10 nm (or larger), grown at high temperature, we have shown here that the shape is a truncated octahedron with a majority of (111) facets, as expected from the Wulff–Kaishew theorem. Nevertheless, if coalescence occurs during growth, the equilibrium shape is not reached, and the particles present a majority of (100) facets. It is important to notice that for a large faceted particle it could be very difficult (sometimes virtually impossible) to reach the equilibrium shape below the melting point [40].

7.2. Adsorption

We have seen an important difference in the adsorption rate of reactants (CO and NO) on supported particles, in comparison with extended surfaces. The adsorption rate increases

with the capture of the reactants physisorbed on the support by the catalyst particles. This phenomenon, called reverse spillover, is not limited to the system studied here; it has also been observed in many other reactions and model catalysts (see [4] for a review on this effect). This effect can increase the adsorption rate by a factor of ten; it becomes more important with decreasing particle size and particle number density.

The adsorption of NO is first molecular, then adsorbed NO can dissociate, if the temperature is sufficiently high and the coverage sufficiently low. The adsorption energy of NO (at low coverage) has been found to be 32 kcal mol^{-1}. This value is in agreement with measurements, in the same range of coverage, on extended Pd(111) [45] and Pd(100) [34]. After dissociation we have seen that two types of adsorbed nitrogen atom coexist on the Pd clusters. The first recombines easily in the temperature window for the reaction (150–450 °C) to form nitrogen molecules, that readily desorb. The second is strongly adsorbed and does not desorb during the reaction and then limits further dissociation of NO. We have observed that the amount of this strongly bound nitrogen species increases with decreasing particle size. Strongly bound nitrogen atoms appear only in the first NO pulses on a fresh sample. After this first exposition to NO (about 10 L) we observe only reversible dissociation corresponding to the loosely bound nitrogen atoms. The reversible dissociation probability of NO was found to depend on both particle size and particle shape. For particle shapes exposing mainly (111) facets it increases with particle size. For the large particles exposing mainly (100) facets the (reversible) dissociation rate decreases relative to the particles with dominating (111) facets. On extended Pd(111) surfaces, NO dissociation does not occur except at defects (presumably steps) [45, 46]. The dissociation barrier has been found to be 27.6 kcal mol^{-1} [45]. On Pd(110) and Pd(320) it is also suggested that dissociation occurs at steps [16, 47]. These results are in agreement with recent DFT calculations showing that the dissociation barrier on smooth Pd surfaces is very high, leading to practically no dissociation, but it is considerably decreased at steps [48, 49]. On Pd particles supported on alumina an increase of the dissociation, when the particle size decreases, has been observed [15, 17, 50] and two peaks, at 260 and 430 °C, were observed in the TPD curves for N_2 associative desorption [15, 50]. The increase of the proportion of the high-temperature desorption peak, when particle size decreases, can be attributed to low-coordination Pd sites. It will correspond to the irreversible dissociation that we observed in our molecular beam experiments. This result, however, is in contradiction with DFT calculations that predict a lower association energy of nitrogen atoms on steps than on smooth (111) and (100) terraces [49].

We have observed, in the temperature range of this study (150–450 °C), that no oxygen desorbs from the sample, in agreement with TPD experiments on extended Pd surfaces showing a desorption peak near 530 °C [30–32]. However, the present experiments show that oxygen atoms resulting from the dissociation of NO diffuse inside the volume of the Pd particles. This result is in line with experiments showing that oxygen can diffuse below the surface of extended Pd(111) [30, 51], (110) [52–54] and (112) [46] surfaces. The diffusion inside the Pd lattice is reversible and it is an activated process; it is easier in the more open surfaces. On supported Pd particles, the diffusion of oxygen atoms inside the particles has been also observed by several authors [55–57] and it was shown that this process was more important in the smaller particles [56]. Considerable amounts of oxygen can be stored in the Pd lattice and this dissolved oxygen is not reactive with CO as long as it remains under the surface [30]. However, the presence of subsurface oxygen reduces the adsorption energy of CO [36].

The observation that the adsorption energy of CO is slightly lower than for NO agrees with DFT calculations that predict a difference of 6% [49].

7.3. NO–CO reaction

It had been proposed [11] that CO reacts directly with NO by the following reaction:

$$CO + NO \rightarrow CO_2 + N_{ad}. \tag{2}$$

However, our measurements (figure 8) show that this reaction does not occur because NO does not react with the surface of a Pd particle covered with CO. Although NO is able to displace CO, no CO_2 was produced. In fact dissociation of NO is a necessary step for the reaction. In the preceding case of a high coverage of CO, there was no room for NO to dissociate and no reaction could occur. The mechanism of the reaction is that already proposed for Rh by Belton [58]:

$$NO \leftrightarrow NO_{ad} \tag{3}$$

$$NO_{ad} \rightarrow N_{ad} + O_{ad} \tag{4}$$

$$N_{ad} + N_{ad} \rightarrow N_2 \tag{5}$$

$$N_{ad} + NO_{ad} \rightarrow N_2O \tag{6}$$

$$CO \leftrightarrow CO_{ad} \tag{7}$$

$$CO_{ad} + O_{ad} \leftrightarrow CO_2. \tag{8}$$

We have to add the diffusion of adsorbed oxygen in the bulk of the Pd particles:

$$O_{ad} \rightarrow O_{bulk}. \tag{9}$$

In our experiments on supported particles reaction (6) is negligible in practice. We have shown previously that the RLS for the reaction is the dissociation of NO at low temperature and the CO adsorption at high temperature [19]. On extended Pd surfaces the branching ratio between reactions (5) and (6) is largely in favour of N_2O for Pd(111), while it is in favour of N_2 for Pd(100) [14]. This is explained by a larger coverage of NO relative to CO on the Pd(111), that would favour reaction (6).

It has been clearly shown by Goodman's group that the (111) surface is more active than the (100), one which itself is more active than the (110) surface [12, 14]. This is at first sight surprising because, if we admit that NO dissociation is a crucial step for the reaction, one would expect that the more open surfaces, which are more efficient for NO dissociation, would be the most active. In fact this apparent contradiction has been solved by Goodman's group. They have shown that the more open surface produces more strongly bound nitrogen, which desorbs at a temperature higher than the maximum of the reaction. In particular, they have clearly shown that during the reaction on Pd(100), 80% of the surface sites were covered by this inactive nitrogen species while only 20% on Pd(111) [14]. In our experiments, the irreversible NO dissociation corresponds to the formation of this inactive nitrogen while the reversible NO dissociation leads to active nitrogen species that desorbs associatively during the reaction. On large particles (45 nm) exposing mainly (100) facets, we have shown previously that the coverage of this inactive nitrogen species was about 80% of a monolayer in the NO adsorption experiments [29].

Results on supported Pd/Al_2O_3 model catalysts show that when particle size is decreasing the activity for the NO-CO reaction drops [15]. Powder catalysts present the same trends but they are even less active than the supported model catalysts [15]. Our experiments have previously shown that the activity of the reaction depends on the particle size but also on the particle morphology [18, 19]. From these studies one can derive the following trends. For particles having the same morphology, the activity (per active site) is expected to be constant for particles larger than about 5 nm. For smaller particles the activity decreases due to an increasing fraction of low-coordination edge sites. For a given particle size, particles exposing

more (111) facets than (100) facets must be more active. Particles presenting a rough surface (i.e. no well developed facets) are expected to show low activity. This can explain qualitatively all the observations on model catalysts from Goodman's group and our group and it further stresses the fact that it is very important to characterize the actual morphology of the metal particles.

Another important remark concerns the measurement of the activity. In catalysis, one compares the activity between different catalysts by comparing the TOF (turnover frequency) that corresponds to the number of molecules produced per second and per active site. These measurements first need the knowledge of the actual morphology of the metal particles. Moreover, the TOF measurements can be misleading. As we have shown, the adsorption of the reactants on the metal particles occurs via two channels: direct impingement and capture of molecules physisorbed on the support. The second channel depends on particle size and particle density. Then the actual adsorption rate of reactants is not directly related to the pressure. For example, if we compare the activity of two samples having different particle sizes the net adsorption rate will be larger on the smaller particles. Then, if the reaction rate increases with the pressure of one reactant, it is not possible to compare the activity between the two catalysts from the TOF measurements. This means that it is first necessary to understand the dependence of the reaction rate on the different partial coverages on monodisperse particles, before comparing particles with different sizes. Here, the small particles will exhibit an increase of the TOF simply because they receive more reactant and not because of an intrinsic higher activity. We have seen (figure 12) that the activity for the CO–NO reaction increased with NO pressure (in the pressure range 10^{-8}–10^{-6} Torr). We had observed that the TOF increased with decreasing particle size [18]. However we had to take into account the higher NO flux joining the smaller particles by the reverse spillover effect. One way to make this correction is to calculate the reaction probability of NO. The reaction probability of NO is obtained by dividing the consumption rate of NO, which is measured by using the molecular beam of NO (this is given by the difference between the steady-state productions of NO at zero CO pressure and during the reaction [18]), by the total flux of NO adsorbing on the metal particles, which is obtained during the adsorption measurements with the molecular beam of NO [29]. Indeed, after this correction the intrinsic activity of the different particles could be compared [19]. The smallest particles (2.8 nm) were less active than particles of 6.9 nm and large particles of 15.6 nm were less active than the 6.9 nm particles because they had coalesced during growth and presented a majority of (100) facets instead of a majority of (111) facets for the two other samples.

8. Conclusion

To close the material gap in heterogeneous catalysis it is possible to work with supported model catalysts prepared by epitaxial growth of metal particles on oxide single crystals. However, to extract valuable information from reactivity studies it is necessary to characterize in detail the model catalysts. It is necessary to know the particle size and density and their structure and morphology. These characterizations can be conveniently undertaken by TEM. AFM and STM can also bring complementary information. The control of the morphology can be reached by growing the metal particles at high temperature in order to obtain the equilibrium shape. In the case of Pd particles, truncated octahedron shapes are obtained.

The reactivity of Pd particles supported on MgO(100) surfaces has been studied by molecular beam methods for the reduction of NO by CO. By these techniques it is possible to study the elementary steps of the reaction and to derive the reaction mechanism. The crucial

step in this reaction is the dissociation of NO. It leads to adsorbed nitrogen and adsorbed oxygen atoms. Two types of nitrogen species are observed: a weakly bound nitrogen that desorbs easily in the reaction temperature window (150–450 °C) and a strongly bound species that does not desorb during the reaction. Adsorbed oxygen reacts with adsorbed CO but it can also diffuse inside the lattice of the Pd particles. The precise determination of the dependence of the reactivity of the catalysts on the pressure of the reactants allows us to compare particles of different characteristics. The reactivity of the Pd clusters depends on their size but also on their shape. The support also plays an important role in the reaction kinetics through the diffusion and the capture, by the Pd particles, of the reactant molecules physisorbed on the support. This reverse-spillover effect depends on the particle density and on the particle size.

From this reaction mechanism it has been possible to undertake a microkinetic modelling of the reaction, that will be presented elsewhere [37]. The size and shape effects evidenced for this reaction are currently modelled by Monte Carlo simulations [59].

References

[1] Somorjai G A 1994 *Introduction to Surface Chemistry and Catalysis* (New York: Wiley)
[2] Che M and Bennet C O 1989 *Adv. Catal.* **36** 55
[3] Campbell C T 1997 *Surf. Sci. Rep.* **27** 1
[4] Henry C R 1998 *Surf. Sci. Rep.* **31** 231
[5] Bäumer M and Freund H J 1999 *Prog. Surf. Sci.* **61** 127
[6] Dellwig T, Rupprechter G, Unterhalt H and Freund H J 2000 *Phys. Rev. Lett.* **85** 776
[7] Beitel G A, Laskov A, Oesterbeek H and Kuipers E W 1996 *J. Phys. Chem.* **100** 12 494
[8] Osterlund L, Rasmussen P B, Thostrup P, Laegsgaard E, Stensgaard I and Besenbacher F 2001 *Phys. Rev. Lett.* **86** 460
[9] Davies P W and Lambert R M 1981 *Surf. Sci.* **1101** 227
[10] Yamada T, Matsuo I, Nakamura T, Xie M, Hirano H, Matsumoto Y and Tanaka K I 1990 *Surf. Sci.* **231** 304
[11] Xi G, Bao J, Shao S and Li S 1992 *J. Vac. Sci. Technol.* A **10** 2351
[12] Vesecky S M, Chen P, Xu X and Goodman D W 1995 *J. Vac. Sci. Technol.* A **13** 1539
[13] Datè M, Okuyama H, Takagi N, Nishijima M and Aruga T 1996 *Surf. Sci.* **350** 79
[14] Vesecky S M, Rainer D R and Goodman D W 1996 *J. Vac. Sci. Technol.* A **14** 1457
[15] Rainer D R, Vesecky S M, Koranne M, Oh W S and Goodman D W 1997 *J. Catal.* **167** 234
[16] Hirsimäki M, Suhonen S, Pere J, Valden M and Pessa M 1998 *Surf. Sci.* **402–4** 187
[17] Xu X and Goodman D W 1994 *Catal. Lett.* **24** 31
[18] Piccolo L and Henry C R 2000 *Appl. Surf. Sci.* **162/163** 670
[19] Piccolo L and Henry C R 2001 *J. Mol. Catal.* A **167** 181
[20] Duriez C, Henry C R and Chapon C 1991 *Surf. Sci.* **253** 190
[21] Henry C R and Meunier M 1998 *Vacuum* **50** 157
[22] Henry C R 1998 *Cryst. Res. Technol.* **33** 1119
[23] Graoui H, Giorgio S and Henry C R 1998 *Surf. Sci.* **417** 350
[24] Müller P and Kern R 2000 *Surf. Sci.* **475** 229
[25] Graoui H, Giorgio S and Henry C R 2001 *Phil. Mag.* B **81** 1649
[26] Ferrero S, Piednoir A and Henry C R 2001 *Nanoletters* **1** 227
[27] Piednoir A, Perrot E, Granjeaud S, Humbert A, Chapon C and Henry C R 1997 *Surf. Sci.* **391** 19
[28] Hansen K H, Worren T, Stempel S, Laegsgaard E, Bäumer M, Freund H J, Besenbacher F and Stensgaard I 1999 *Phys. Rev. Lett.* **83** 4120
[29] Piccolo L and Henry C R 2000 *Surf. Sci.* **452** 198
[30] Leisenberger F P, Koller G, Sock M, Surnev S, Ramsey M G, Netzer F P, Klötzer B and Hayek K 2000 *Surf. Sci.* **445** 380
[31] Ertl G and Koch J 1970 *Z. Phys. Chem.* **69** 323
[32] Yagi K, Sekiba D and Fukutani H 1999 *Surf. Sci.* **442** 307
[33] Henry C R, Duriez C and Chapon C 1991 *J. Chem. Phys.* **95** 700
[34] Yeo Y Y, Vattuone L and King D A 1997 *J. Chem. Phys.* **106** 1990
[35] Henry C R, Chapon C, Goyhenex C and Monot R 1992 *Surf. Sci.* **272** 283
[36] Ladas S, Imbihl R and Ertl G 1993 *Surf. Sci.* **280** 14

[37] Prévot G and Henry C R submitted
[38] Zhdanov V P and Kasemo B 1997 *Surf. Sci. Rep.* **29** 31
[39] Wulff G 1901 *Z. Kristallogr.* **34** 449
[40] Henry C R *Catalysis of Nanoparticle Surfaces* ed A Wiecowski *et al* (New York: Dekker) at press
[41] Hansen P L and Wagner J B *EUREM 12 Proc. (Brno, 2000)* vol 2 p 537
[42] Erlandsson R, Eriksson M, Olsson L, Helmersson U, Lundström I and Pettersson L G 1991 *J. Vac. Sci. Technol.* B **9** 825
[43] Renaud G 1998 *Surf. Sci. Rep.* **32** 1
[44] Kaishew R 1952 *Arbeitstagung Festkörper Physik* (Dresden) p 81
[45] Schmick H D and Wassmuth H W 1982 *Surf. Sci.* **123** 471
[46] Ramsier R D, Gao Q, Neergaard Waltenburg H, Lee K W, Nooij O W, Leffert L and Yates J T 1994 *Surf. Sci.* **320** 209
[47] Sharpe R G and Bowker M 1996 *Surf. Sci.* **360** 21
[48] Loffreda D, Simon D and Sautet P 1998 *J. Chem. Phys.* **108** 6447
[49] Hammer B 2001 *J. Catal.* **199** 171
[50] Cordatos H, Bunluesin T and Gorte R J 1995 *Surf. Sci.* **323** 219
[51] Zheng G and Altmann E I 2000 *Surf. Sci.* **462** 151
[52] He J W and Norton P R 1988 *Surf. Sci.* **204** 26
[53] Ladas S, Imbihl R and Ertl G 1989 *Surf. Sci.* **219** 88
[54] Bondzie V A, Kleban P and Dwyer D J 1996 *Surf. Sci.* **347** 319
[55] Stara I, Nehasil V and Matolin V 1996 *Surf. Sci.* **365** 69
[56] Putna E S, Vohs J M and Gorte R J 1997 *Surf. Sci.* **391** L1178
[57] Meusel I, Hoffman J, Hartmann J, Heeimer M, Bäumer M, Libuda J and Freund H J 2001 *Catal. Lett.* **71** 5
[58] Permana H, Ng K Y S, Peden C H F, Schmieg S J, Lambert D K and Belton D N 1996 *J. Catal.* **164** 194
[59] Bustos V, Unac R O, Zgrablich G and Henry C R, to be published